USING COMPUTATIONAL FLUID DYNAMICS TO PREDICT HEAD LOSSES IN THE AUXILIARY ELEMENTS OF A MICROIRRIGATION SAND FILTER

G. Arbat, T. Pujol, J. Puig-Bargués, M. Duran-Ros, J. Barragán, L. Montoro, F. Ramírez de Cartagena

ABSTRACT. *It is often assumed that total head losses in a sand filter are solely due to the filtration media and that there are analytical solutions, such as the Ergun equation, to compute them. However, total head losses are also due to auxiliary elements (inlet and outlet pipes and filter nozzles), which produce undesirable head losses because they increase energy requirements without contributing to the filtration process. In this study, ANSYS Fluent version 6.3, a commercial computational fluid dynamics (CFD) software program, was used to compute head losses in different parts of a sand filter. Six different numerical filter models of varying complexities were used to understand the hydraulic behavior of the several filter elements and their importance in total head losses. The simulation results show that 84.6% of these were caused by the sand bed and 15.4% were due to auxiliary elements (4.4% in the outlet and inlet pipes, and 11.0% in the perforated plate and nozzles). Simulation results with different models show the important role of the nozzles in the hydraulic behavior of the sand filter. The relationship between the passing area through the nozzles and the passing area through the perforated plate is an important design parameter for the reduction of total head losses. A reduced relationship caused by nozzle clogging would disproportionately increase the total head losses in the sand filter.*

Keywords. *Clogging, Computational fluid dynamics, Drip irrigation, Filtration, Flow simulation, Models, Nozzle, Underdrain.*

Emitter clogging is a major problem in microirrigation systems, especially when using low-quality water (Ravina et al., 1997). Drip emitters have outlets ranging from 0.3 to 0.7 mm, and, as a general rule, filtration systems must remove particles larger than 1/10th the diameter of the emission orifice to prevent emitter plugging (Burt and Styles, 2007). To protect emitters, screen, disc, and sand filters are all commonly used, but sand filtration is often considered the standard for filtration protection of microirrigation systems (Trooien and Hills, 2007). The sand media sizes usually used range from 0.46 to 0.79 mm, providing filtration of particles between 0.040 to 0.075 mm (Nakayama et al., 2007). In practice, the concept of an effective media size (d_{10}, referring to the size of the smallest 10% of the particles) is commonly used. Burt and Styles (2007) justified the use of effective diameter, arguing that during backwashing the finer particles tend to migrate toward the top of the bed, where they settle and perform the majority of the filtration. Another important parameter is the sand uniformity coefficient (UC), which is defined as the ratio of the size opening through 60% of the sand will pass to the size opening through which 10% will pass (AWWA, 2001).

Head loss in a sand filter, which depends on the size of the filter media, is higher when the media size is finer. However, head losses in a filter are not restricted to the filter media, as there are also head losses in the inlet and outlet pipes, the filter underdrain (nozzles), and other components of the filter. Burt (2010) experimentally determined head losses in the nozzles, sand, and backflush valves in three different commercial filters of 1219 mm nominal diameter with a nozzle-type underdrain, operating at flow rates ranging from 2040 to 4380 $m^3 h^{-1}$. The results showed that the head losses in the nozzles and backflush valves could be greater than the head losses produced by the sand media. Changes in commercial filter configuration may also substantially modify the total head losses (Burt, 2010).

The filtration process is produced in the sand media, and even though other filter components are needed for proper functioning, head losses in the auxiliary elements must be minimized in order to reduce energy requirements. Moreover, partial clogging at the filter nozzles can increase undesirable head losses. Thus, Fahjen (1995) and Barth (1995) reported that clogging or damage to the filter nozzles can cause the filter to malfunction.

Yurdem et al. (2008), using dimensional analysis techniques, developed equations to compute head losses in microirrigation disc filters. The equations were useful in predicting the head losses for different operational conditions and filter designs. Puig-Bargués et al. (2005) and Duran-Ros et al. (2010) used the same technique to develop equations to

Submitted for review in February 2011 as manuscript number SW 9043; approved for publication by the Soil & Water Division of ASABE in July 2011.

The authors are **Gerard Arbat,** Assistant Professor, Department of Chemical and Agricultural Engineering and Technology, **Toni Pujol,** Associate Professor, Department of Mechanical Engineering and Industrial Construction, **Jaume Puig-Bargués,** Associate Professor, Department of Chemical and Agricultural Engineering and Technology, and **Miquel Duran-Ros,** Assistant Professor, Department of Chemical and Agricultural Engineering and Technology, University of Girona, Girona, Spain; **Javier Barragán,** Professor, Department of Agricultural and Forestry Engineering, University of Lleida, Lleida, Spain; **Lino Montoro,** Assistant Professor, Department of Mechanical Engineering and Industrial Construction, and **Francisco Ramírez de Cartagena,** Associate Professor, Department of Chemical and Agricultural Engineering and Technology, University of Girona, Girona, Spain. **Corresponding author:** Gerard Arbat, Department of Chemical and Agricultural Engineering and Technology, University of Girona, C. de Maria Aurèlia Campany 61, 17071 Girona, Spain; phone: +34972418459; email: gerard.arbat@udg.edu.

  ISSN 2151-0032

predict head losses when using sand, disc, and screen filters to filter effluents of different quality. Their results highlighted the influence of water quality, regardless of the filter being used.

Dimensional analysis has been shown to be a useful technique for the development of equations to predict head losses in drip irrigation filters, but its use has important constraints. First, it requires a great deal of experimental data; second, the scope of the equations is limited to the previously tested experimental conditions; and third, it does not provide a physical explanation of the filtration process.

Computational fluid dynamics (CFD) seems to be a promising technique to overcome these limitations. It solves the hydrodynamic equations by taking into account a given filter geometry while also permitting visualization of the inner velocity field within the different filter components. Ortiz-Arroyo et al. (2002) formulated a *k*-fluid Eulerian 2D transient CFD model to describe the space-time evolution of clogging patterns developing in bed filtration of liquids. Among other uses, CFD modeling has been applied to the evaluation of the hydraulic performance of drip emitters (Wei et al., 2006), to the computation of local losses of emitters (Palau-Salvador et al., 2006) and laterals (Provenzano et al., 2007), to the prediction of discharge variation due to clogging in drip irrigation emitters (Qingsong et al., 2008), and to the study of filtration performance of air filters (Qian and Wang, 2010).

The main objective of this study has been to analyze the hydraulic behavior of the auxiliary elements (inlet and outlet pipes and filter nozzles) in a pressurized sand filter using CFD software.

Material and Methods

Experimental Layout

A sand filtration unit with two parallel sand filters, both 500 mm internal diameter and with a filtration surface of 1963 cm^2, was used for a drip irrigation system. Each sand filter was filled with approximately 175 kg of silica sand in a single filtration layer. The effective sand size (d_{10}) was 0.47 mm, and the sand uniformity coefficient (UC) was 1.81. The porosity of the sand (ε), defined as the volume of voids divided by the volume of the packed bed region, was 0.375, and the sand bed height (L_s) was 0.57 m. At the base of the sand there was a perforated metallic plate with 12 drill-holes 16 mm in diameter. A perforated nozzle was screwed into each drill-hole to prevent sand loss. Each nozzle had 45 slots, 0.45 mm wide and 30 mm long, with a total passing surface of 7.29×10^3 mm^2, considering the 12 nozzles of the filter. The main dimensions of the filter in a plane cut through the centerline of both the inlet and outlet pipes are shown in figure 1. Nozzle distribution on the perforated plate is shown in figure 2.

The water flow at the filtration unit was measured using an MP400CB electromagnetic flowmeter, with a measurement range from 2 to 20 $m^3\ h^{-1}$ and an accuracy of ±1% (Comaquinsa, Llinars del Vallès, Spain). The pressure was measured at the filter inlet collector (p_{in} in fig. 3) and at an outlet derivation (p_{out} in fig. 3) with an MBS 4010 pressure transmitter with flush diaphragm, a measurement range of 0 to 600 kPa, and an accuracy of ±0.3% (Danfoss, Nordborg, Denmark). Flow rate and pressure were collected every minute by a supervisory control and data acquisition system (SCADA) previously developed (Duran-Ros et al., 2008). The tertiary effluent from the wastewater treatment plant (WWTP) of Celrà (Girona, Spain) was used in the experiments. Additional details concerning water quality are provided by Puig-Bargués et al. (2010).

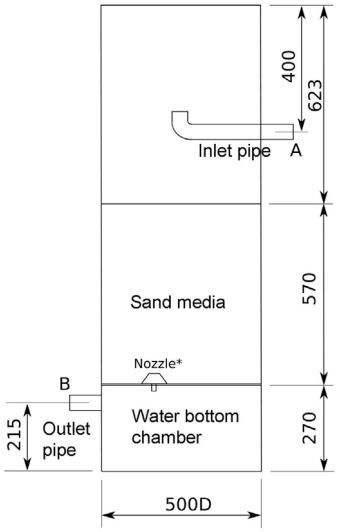

Figure 1. Cross-section of the sand filter through the centerline of both the inlet and outlet pipes (units in mm). Both inlet and outlet pipe diameters are 50.8 mm. *A single nozzle is shown here for illustrative purposes only, since nozzles do not appear in a cross-sectional view of the actual filter (see nozzle distribution in fig. 2).

Operational Procedure

The experiment was conducted over 540 h between August 3 and December 7, 2007, although there was a break after 107 h of irrigation, from August 24 to October 4, when the treatment plant did not supply any tertiary effluent. Operation time varied between 6 and 12 h per day, with minor interruptions of a few days primarily due to operational problems and system maintenance. The sand filters were backwashed automatically for 90 s when the pressure head loss across them was higher than 50 kPa.

In order to establish initial conditions in the CFD simulations, ten filtration cycles from among the 117 carried out were selected. Only ten were selected mainly because each filtration cycle needed to be analyzed in depth to remove strange data, especially that collected at the beginning of each cycle, immediately after automatic backwashing of the filter when inlet and outlet pressures were increasing somewhat erratically due to the effect of opening and closing valves. Short filtration cycles and cycles with high and/or abrupt pressure drops during the cycle were also eliminated from the analysis.

The duration of the selected cycles ranged from 160 to 442 min. The mean measured inlet (p_{in}) and outlet (p_{out}) pressures (± standard deviation) during the initial 5% of the cycle time were 476.0 kPa (±8.5 kPa) and 441.5 kPa (±8.7 kPa), respectively. The mean pressure head difference considering p_{in} and p_{out} was 34.5 kPa (±2.6 kPa). The mean water flow (± standard deviation) at the filtration unit was 10.87 $m^3\ h^{-1}$ (±0.20 $m^3\ h^{-1}$). As the filtration unit was composed of two sand filters of identical characteristics connected in parallel, the water flow through a single filter was assumed to be half of the total flow.

Figure 2. View of nozzle distribution on the perforated plate located at the bottom of the sand bed.

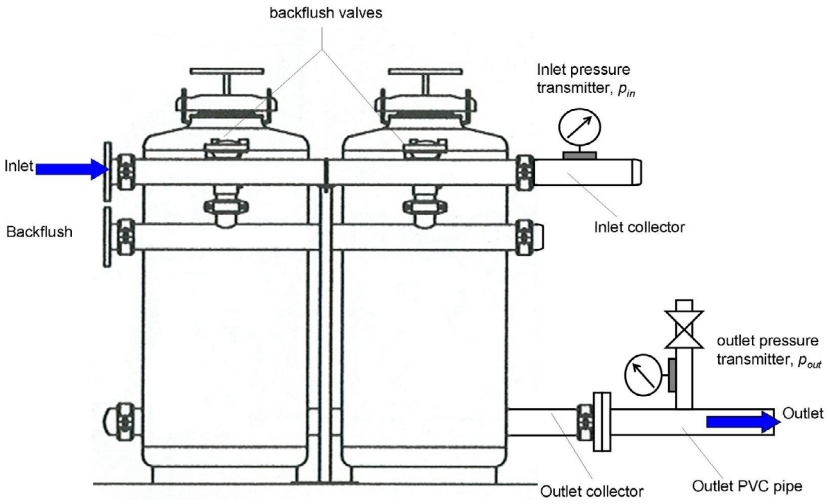

Figure 3. Pressure measurement locations of inlet and outlet pressures (p_{in} and p_{out}).

The mean inlet (p_A) and outlet (p_B) filter pressures (points A and B in fig. 1) were calculated taking into account the head losses due to the pipes between points A and B and the inlet and outlet pressure transmitters (p_{in} and p_{out}), as well as the head losses due to the backflush valve (Flushgal 2", Regaber, Parets del Vallès, Spain) (fig. 3). Major losses due to friction effects (Δp_M) follow from the Darcy–Weisbach equation:

$$\Delta p_M = \rho f \frac{L}{d^5} \frac{8Q^2}{\pi^2} \quad (1)$$

where ρ is the fluid density (kg m^{-3}), Q is the volumetric flow rate (m^3 s^{-1}), f is the friction coefficient, and L and d are the pipe length and diameter, respectively (m).

Minor losses (Δp_m) follow from White (2008):

$$\Delta p_m = \rho \zeta \frac{8Q^2}{d^4 \pi^2} \quad (2)$$

where ζ is the minor loss coefficient.

Equation 1 applied to the inlet collector, 265 mm long (fig. 3), produced a major head loss (Δp_M) of 93 Pa since the friction coefficient (f) of 0.064 follows from the Moody chart once we apply the roughness value (2 mm) corresponding to a rusted steel duct (as experimentally observed) (White, 2008). Equation 2 produced a minor head loss (Δp_m) of 336 Pa when minor loss coefficients (ζ) of 1 for the tee and 0.211 for contraction from the collector (72 mm inside diameter) to the filter inlet pipe (50.8 mm inside diameter) were considered (White, 2008). Taking into account the flow rate for a single filter (5.43 m^3 h^{-1}), the backflush valve produced a head loss equal to 1669 Pa (Flushgal 2", Regaber, Spain). Therefore, total head losses from the filter inlet (point A in fig. 1) to the position where p_{in} was measured (fig. 3) were 2098 Pa, and p_A = 476.0 – 2.1 = 473.9 kPa.

Equation 1 applied to the outlet collector, 350 mm long and 71 mm inner diameter (fig. 3), produced a major head loss (Δp_M) of 74 Pa, since f = 0.055 (roughness value approxi-

mately equal to 2 mm; White, 2008), and equation 1 applied to the outlet PVC pipe, 250 mm long and 50.8 mm inner diameter, produced a major head loss (Δp_M) of 106 Pa, since f = 0.0195 (roughness value approximately equal to 0.0015 mm; White, 2008). Equation 2 produced a minor head loss (Δp_m) of 2734 Pa when minor loss coefficients (ζ) of 2 for the tee (Mataix, 1982), 0.252 for stretching from the filter outlet to the outlet collector (White, 2008), and 0.211 for contraction from the collector to the PVC pipe (White, 2008) were used. Therefore, total head losses from the filter outlet (point B in fig. 1) to the position where p_{out} was measured (fig. 3) were 2914 Pa.

Total head losses from the filter inlet and outlet (p_A and p_B) to the respective measured points (p_{in} and p_{out}) would be 5012 Pa; therefore, the mean pressure head difference considering p_A and p_B would be 29.5 kPa (±2.6 kPa).

Filter Models

Analytical Models

Several elements contribute to the total head loss ($\Delta p_t = p_A - p_B$) measured in the filter, classified here as porous media (sand) and auxiliary elements. The latter corresponds to inlet and outlet pipes, the perforated plate, and the nozzles.

Two analytical models were used. The ASP model takes into account head losses due to sand media as well as friction effects in both inlet and outlet pipes, whereas the ASPP model adds to these elements the contribution of the perforated plate located below the sand column (table 1). The effect of nozzles was not taken into account since an analytical model for such elements is not available. Expressions for evaluating the pressure decrease in each of the above elements are shown below.

Sand Media

The Ergun expression (Macdonald et al., 1979) was used to obtain head losses through the sand media (Δp_s):

$$\Delta p_s = L_s \left[\frac{150\mu}{{d_{10}}^2} \frac{(1-\varepsilon)^2}{\varepsilon^3} \frac{4Q}{\pi D^2} + \frac{1.75\rho}{d_{10}} \frac{(1-\varepsilon)}{\varepsilon^3} \frac{16Q^2}{\pi^2 D^4} \right] \quad (3)$$

where L_s is the sand bed height (m), d_{10} is the effective sand size (m), ε is the porosity, μ is the fluid viscosity (Pa s), and D is the filter diameter (m). Using the values corresponding to the Experimental Layout section, equation 3 gives Δp_s = 23.3 kPa.

In the original Ergun equation, mean grain size (d_{mean}) was used instead of effective grain size (d_{10}); however, in practice d_{10} is the usual way to specify media size. Burt and Styles (2007) justified the use of d_{10} by arguing that during backwashing the finer particles tend to migrate toward the top of the bed, where they settle and provide the majority of the filtration.

Auxiliary Elements: Inlet and Outlet Pipes

Both major and minor head losses contribute to total head losses in the inlet and outlet pipes. Major losses due to friction effects (Δp_M) follow from the Darcy-Weisbach equation (eq. 1), and minor losses (Δp_m) follow from White (2008) (eq. 2).

Equations 1 and 2 applied to the inlet pipe (fig. 1) produced a head loss of Δp_i = 586 Pa when the minor loss coefficients were ζ = 0.64 for elbows and ζ = 1 at the pipe exit (White, 2008), and an inlet pipe length of 390 mm was used. Roughness values correspond to those employed in the Operational Procedure section. For the outlet pipe, equations 1 and 2 predicted a total head loss of only Δp_o = 174 Pa, since the minor loss coefficient was ζ = 0.50 at the pipe entry and the outlet pipe length was 100 mm. Thus, the total head loss analytically predicted for both inlet and outlet pipes corresponds to Δp_p = 760 Pa, and the total head loss for the ASP model is therefore $\Delta p_t = \Delta p_s + \Delta p_p$ = 24.1 kPa.

Auxiliary Elements: Perforated Plate

The perforated plate above the sand bed includes holes 16 mm in diameter and 25 mm long, with a center-to-center distance in the order of 100 mm. This gives us values for the hole pitch-to-diameter ratio and for the plate free area that lie outside those applied in the studies of discharge coefficients through perforated plates to predict head losses (e.g., Smith and van Winkle, 1958). Equations 2 and 3 were therefore applied to derive the head loss through the perforated plate, giving Δp_{pp} = 391 Pa, meaning that total head loss for the ASPP model was $\Delta p_t = \Delta p_s + \Delta p_p + \Delta p_{pp}$ = 24.4 kPa. Note that in both the ASP and ASPP analytical models, head losses derived individually for each of the elements (sand, pipes, and perforated plate) were added together. However, in the real filter, the elements influence each other (especially the perforated plate and the sand media), so analytical head losses are not expected to correctly reproduce real filter behavior.

Numerical Models

As stated previously, the severe limitations of analytical models can be overcome by using a numerical model to study the exact filter configuration by numerically simulating fluid dynamics. Here, simulations are performed by means of the general-purpose commercial CFD program ANSYS Fluent, version 6.3 (Fluent, 2009), which has recently been used to study flow through porous media (Zaman and Jalali, 2010) and flow in drippers (Qingsong et al., 2008).

For purposes of comparison with the analytical filter models, simulations of the entire filter domain with the same elements as those used in the analytical versions ASP (sand and pipes) and ASPP (sand, pipes, and perforated plate) were carried out, called here NSP and NSPP, respectively (table 1). In addition, simulations of the entire filter domain including nozzles were performed (NSPPN in table 1). As explained in the Operational Procedure section, several experimental filtration cycles were used to verifying the results of the $NSPPN_a$ model.

As pointed out in Experimental Layout section, the actual nozzles not only consist of very tiny slots but also show a remarkable geometrical complexity in their inner part. A virtual simulation of the actual filter configuration requires a high

Table 1. Elements considered in each model used to predict head losses in the sand filter.

	Analytical		Numerical[a]			
Filter Element	ASP	ASPP	NSP	NSPP	$NSPPN_s$	$NSPPN_a$
Sand media	x	x	x	x	x	x
Inlet/outlet pipes	x	x	x	x	x	x
Perforated plate	--	x	--	x	x	x
Nozzles	--	--	--	--	x	x

[a] $NSPPN_s$: Each nozzle has 20 slots, and each slot has an area of 30.4 mm^2 (simplified nozzle). $NSPPN_a$: Each nozzle has 45 slots, and each slot has an area of 13.5 mm^2 (actual nozzle).

level of computational resources that, although feasible (see $NSPPN_a$ in table 1), becomes inappropriate when investigating filter behavior under several different working conditions. This is why a simplified version of the filter was devised, consisting of cylindrical nozzles containing the same water volume as the actual nozzles. In this version, a single nozzle contains 20 slots, each 1.0125 mm wide × 30 mm long = 30.375 mm^2 surface area, which gives us the same open area per nozzle as the actual nozzle. As will be discussed in the Results and Discussion section, results simulated with such a simplified configuration ($NSPPN_s$ in table 1) are very similar to those obtained with the actual configuration, while requiring much less computational time. Numerical studies focusing on different nozzles and nozzle clogging were therefore carried out with simplified filter versions. Table 1 summarizes the filter models analyzed here.

The effect of clogging was simulated by reducing the number of slots in the different nozzles to achieve a reduction in the open area of the nozzles. Thus, 50%, 66%, and 75% reductions in area were tested in the numerical simulations. A new nozzle design was also tested by increasing by 50% the number of slots in comparison with the $NSPPN_s$ model, and therefore increasing the ratio between the passing area through the nozzle slots and the passing area through the perforated plate from 3:1 to 4.5:1.

Model Equations

The fluid flow was modeled by numerically solving the conservation equations of mass (continuity equations) and linear momentum for an incompressible fluid (Navier–Stokes equations) with constant density (ρ = 1000 kg m^{-3}) and viscosity ($\mu = 1.003 \times 10^{-3}$ Pa s). The flow through the homogeneous porous media was modeled by adding a momentum source term (S_i) to the standard Navier–Stokes equations, consisting of two parts: a viscous loss term and an inertial loss term (Fluent, 2009):

$$S_i = -\left(\frac{\mu}{\alpha} v_i + C_2 \frac{1}{2} \rho |v| v_i \right) \text{ for } i = x, y, z \tag{4}$$

where v_i and $|v|$ are the ith component and magnitude of the fluid velocity for a sandless filter, respectively (m s^{-1}), α is the permeability (m^2), and C_2 is the inertial resistance factor (m^{-1}). Here, these last two parameters follow from:

$$\alpha = \frac{{d_{10}}^2}{150} \frac{\varepsilon^3}{(1-\varepsilon)^2} \tag{5a}$$

$$C_2 = \frac{3.5}{d_{10}} \frac{(1-\varepsilon)}{\varepsilon^3} \tag{5b}$$

Note that with equations 5a and 5b, equation 4 reverts to the well known Ergun equation (eq. 3), with S_i being the pressure gradient. As usual in porous media simulations, a laminar regime within the region occupied by sand was specified since the flow Reynolds number (Re) in the porous media (Macdonald et al., 1979) is well below the critical value:

$$\mathrm{Re} = \frac{\alpha C_2 \rho v_i}{\mu} \tag{6}$$

All other regions (flow in both the inlet and outlet pipes is obviously turbulent) use the realizable k–e two–layer turbulence model that solves two evolution equations to predict the turbulent kinetic energy (k) and the turbulent dissipation rate (e).

Numerical Algorithms

Fluent code is based on the finite volume method (FVM), which requires a discretization of the domain into small cells. For each cell, the numerical algorithm applied a second–order upwind scheme in all the evolution equations except for pressure, where the linear method was chosen. For the whole computational grid (or mesh), the set of algebraic equations was solved with an adaptive multigrid solver (AMG), in which the SIMPLE algorithm was applied to couple the mass and Navier–Stokes equations (Fluent, 2009).

Steady simulations applied boundary conditions that followed the mean experimental values detailed in the Experimental Layout section. Thus, inlet pressure at inlet surface A (fig. 1) was fixed at 473.9 kPa, whereas at outlet surface B (fig. 1) the outlet mass flow rate was assumed to be 1.51 kg s^{-1}. For both A and B surfaces, a fixed value of turbulent intensity, I = 0.1, was fixed, and the ratio between fluid turbulent viscosity (μ_T) and fluid viscosity (μ) was fixed to be equal to 10, as usual in water flow simulations (e.g., Pujol et al., 2010). It should be pointed out that changes in both turbulent intensity and the ratio between fluid turbulent viscosity (μ_T) and fluid viscosity (μ) values would only slightly modify head losses in the nozzles and pipes, since the flow regime was laminar in the sand media. Therefore, very small changes in the total head loss are expected due to variations of these parameters.

Mesh

All numerical solutions shown in table 1 made use of unstructured meshes, since these allowed greater refinement in the regions of interest (inlet and outlet pipes, plate orifices, and nozzles). The mesh geometric growth rate was smaller than 20% to ensure a high–quality transition between elements of different size. Figure 4 shows the unstructured mesh of 1.9×10^6 elements used for each nozzle in the $NSPPN_s$ model. In order to properly report the discretization error, mesh sensitivity tests for the NSP, NSPP, and NSPPN models were performed in which the inlet–outlet pressure difference (Δp_t) was selected as the key variable. For each case, Δp_t had to be obtained with three significantly different sets of grids. For the NSP model, fine, regular, and coarse meshes, with characteristic sizes of tetrahedral elements for the sand volume of 15, 21, and 30 mm, respectively, were analyzed. This gave the number of elements N_1, N_2, and N_3 in the sand volume reported in table 2.

In contrast with the NSP model, in the NSPP model orifices provided most of the head losses. Therefore, N_1, N_2, and N_3 values for this second mesh sensitivity study were linked to the number of hexahedral elements employed to represent the volume of a single orifice with characteristic sizes of 1 mm (fine mesh), 1.3 mm (regular mesh), and 1.9 mm (coarse mesh), respectively. Finally, the discretization error for the $NSPPN_s$ model was reported by analyzing grids with different numbers of elements per nozzle (N_1, N_2, and N_3), as shown in table 2. In this case, the orifices were meshed with hexahedra with a characteristic size of 1 mm. The NSPP and $NSPPN_s$ meshes used tetrahedra with characteristic sizes of 15 mm for the sand volume and for the water volumes above and below it. In all cases, the mesh at both the inlet and outlet pipes used hexahedral

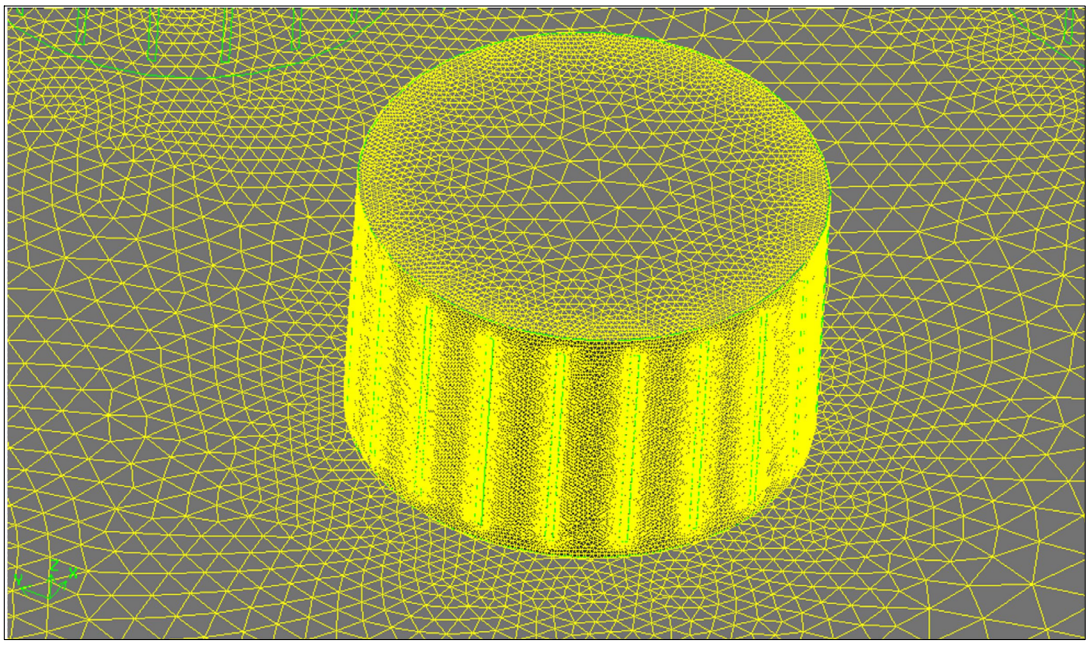

Figure 4. Surface mesh of one cylindrical nozzle and part of the perforated plate in the NSPPN$_s$ model. The finer elements are located in the vertical nozzle slots.

Table 2. Discretization errors measured as a fine grid convergence index (GCI$_{fine}^{21}$) for the NSP, NSPP, and NSPPN$_s$ models, using three different meshes (N_1, N_2, and N_3) for each model.

		Mesh		
Model	Parameter	N_1	N_2	N_3
NSP	No. of elements in sand media	255180	91423	29301
	Δp_t (Pa)	24494	24501	24505
	GCI$_{fine}^{21}$ (%)		0.09	
NSPP	No. of elements for each orifice	6235	2836	1392
	Δp_t (Pa)	82686	83957	85453
	GCI$_{fine}^{21}$ (%)		5.99	
NSPPN$_s$	No. of elements for each nozzle	1.9×10^6	7.2×10^5	3.8×10^5
	Δp_t (Pa)	26767	26848	26937
	GCI$_{fine}^{21}$ (%)		0.41	

elements with a characteristic size of 5 mm. The NSPPN$_a$ mesh used the finer grid configuration of the NSPPN$_s$ mesh detailed above. This gave a total amount of 36×10^6 volume elements for the NSPPN$_a$ model and 26×10^6 volume elements for the simplified NSPPN$_s$ version.

Results and Discussion

Mesh Sensitivity Analysis in Head Loss Predictions

The results for Δp_t shown in table 2 were obtained after averaging the values of the last 500 iterations once the simulations had converged (all residuals were below 5×10^{-4} and did not substantially vary as a function of the iteration). It usually required 6000 iterations to achieve these convergence requirements, in which the standard deviation of the last 500 iterations was below 2 Pa for the Δp_t values shown in table 2. With the above data, the fine grid convergence index (GCI$_{fine}^{21}$) as defined by Celik et al. (2008) was here adopted to account for discretization errors with values less than 6% in all cases.

Head Loss Prediction Using Different Filter Models

The simulated total head losses (Δp_t) for the different numerical models when d_{10} was taken into account are shown in figure 5. The measured head losses were 29.5 ±2.6 kPa, while the predicted losses with most of all the models were slightly lower (fig. 5). NSPPN$_a$ was the filter model that predicted results closest to the experimental data, with 27.1 kPa, 8% smaller than the measured value. However, it should be pointed out that while experimental results were obtained using tertiary effluent as described in the Experimental Layout section, fresh water was considered in the simulations. In consequence, it is to be expected that the experimental head losses would be slightly higher than the predicted values.

The NSPPN$_s$ model predicted a value of Δp_t equal to 26.8 kPa, 9% lower than the measured value. The ASP and NSP models predicted a very similar value of Δp_t (24.1 kPa

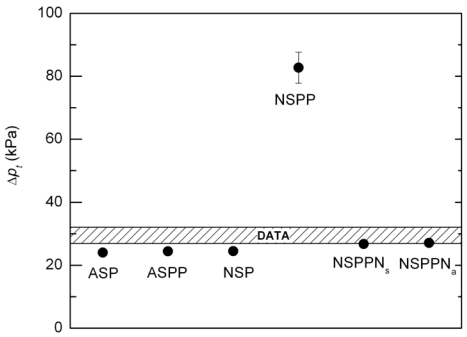

Figure 5. Total head losses (Δp_t) for each filter model and for experimental data (gray range includes ± one standard deviation). Error bars for simulations make reference to the discretization errors detailed in table 2 and were only noticeable in the NSPP model).

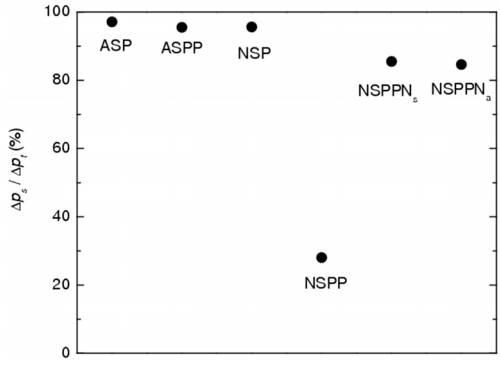

Figure 6. Relationship between the head losses in the sand media (Δp_s) and the total head losses (Δp_t) for each filter model.

for ASP; 24.5 kPa for NSP), as both models are based on the Ergun equation for predicting head losses in sand media, and both take into account head losses in the auxiliary elements (inlet and outlet pipes). On the other hand, the ASPP model gave a slightly greater value of Δp_t than that predicted with the ASP and NSP models, since head losses in the perforated plate were added to the ASP model (see Analytical Models section). In contrast, the NSPP model predicted a significantly higher value of Δp_t than any other model or experimental data (fig. 5), since the perforated plate greatly affects the velocity field inside the sand bed, as we will explain later.

The ratio between head losses in the sand media and the total head losses ($\Delta p_s/\Delta p_t$) is shown in figure 6, where Δp_s is calculated as the area-weighted average pressure at the top of the sand filter minus the area-weighted average pressure at the bottom of the sand filter. In the most realistic filter model (NSPPN$_a$), the ratio $\Delta p_s/\Delta p_t$ was 84.6%, meaning that 15.4% of the total head losses were caused by the auxiliary elements (outlet and inlet pipes, perforated plate, and nozzles) and were therefore of no help in the filtration process.

The NSP model predicted a $\Delta p_s/\Delta p_t$ ratio of 95.6%, which allows us to determine that 4.4% of the head losses were due to the inlet and outlet pipes. By combining the results of the NSPPN$_a$ and NSP sand filter models, we can see that the head losses in the nozzles and the perforated plate can be computed as 15.4% – 4.4% = 11.0% of the total head losses. Burt (2010) showed that head losses in three different commercial filters (1219 mm nominal diameter) using nozzle-type underdrain ranged from 26% to 40%. The greater proportion of head losses in the underdrain can be explained because the filters tested by Burt (2010) were wider and had a larger number of nozzles than the filter studied in this article.

Predicted total head losses (Δp_t) and the $\Delta p_s/\Delta p_t$ ratio (figs. 5 and 6) were very close when using the NSPPN$_s$ and NSPPN$_a$ models. We can therefore say that the simplified nozzles had a similar hydraulic behavior to that of the real nozzles, and that the simplification significantly reduced the simulation time. On the other hand, the NSPP filter model resulted in a significantly greater Δp_t (fig. 5) and a significantly smaller $\Delta p_s/\Delta p_t$ ratio (fig. 6). This shows that there is a very different hydraulic behavior when the filter nozzle is added to the model. It must be noticed that the extremely smaller $\Delta p_s/\Delta p_t$ ratio for the NSPP model was explained by two different reasons. The first reason is in how Δp_s was calculated; as most of the head losses take place in

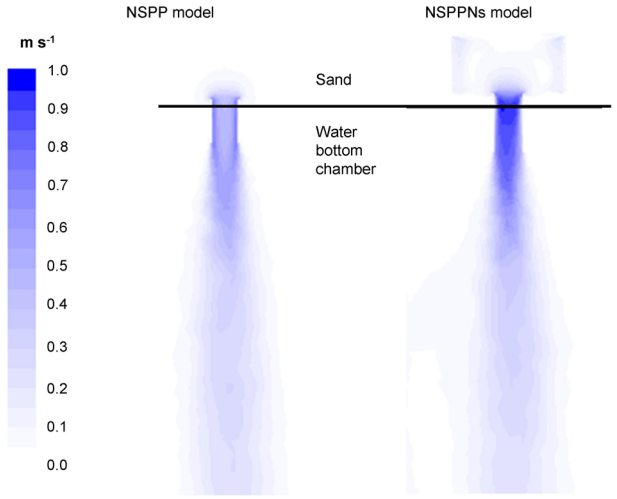

Figure 7. Velocity magnitude (m s^{-1}) in a vertical cross-section through the tube (NSPP model) and nozzle symmetry plane (NSPPN$_s$ model). The horizontal line corresponds to the upper part of the perforated plate. Above this line is the sand media; below this line is the bottom of the filter chamber.

a tiny area over the perforated plate (fig. 9), when the area-weighted average pressure at the bottom of the sand filter was calculated, this gave as a result a reduced Δp_s value. The second reason is that the Δp_t value in the NSPP model was greater than in the other filter models.

The noticeably different hydraulic behavior between NSPP and the other filter models is because the presence of the perforated plate modifies the velocity field to a greater extent than is the case when only the sand media is considered (the NSP model) or when the nozzles are taken into account (the more complex NSPPN$_s$ and NSPPN$_a$ models). In figure 7, velocity magnitude in a vertical plane that cuts one tube (NSPP) or one nozzle (NSPPN$_s$) by its symmetry plane is depicted, showing a bigger region with higher velocities in the sand media for the NSPP model. This meant that head losses computed with the Ergun equation within the sand region close to the orifice were extremely high for the NSPP model. Nevertheless, the average value of the static pressure in the bottom layer of the sand media was essentially the same as that obtained with the NSP, NSPPN$_a$, and NSPPN$_s$ models.

It is important to stress that the presence of the nozzles also modified the velocity field, as can be seen for the NSPP and NSPPN$_s$ models in figure 8. In the NSPP model, the velocity within the tubes in the perforated plate reached 0.70 m s^{-1}, while in the NSPPN$_s$ model higher values for the velocity magnitude (up to 1.00 m s^{-1}) were found, with the same mass flow rate for both cases. This implies a rather different velocity profile within the tubes for both the NSPP and NSPPN$_s$ models, mainly caused by differences in the pressure field, as explained below. In the NSPPN$_s$ model, the mean velocity perpendicular at the nozzle slot was 0.21 m s^{-1}, while at the entrance of the tubes the velocity magnitude increased to 0.73 m s^{-1}, with its mean perpendicular component being 0.63 m s^{-1}. The latter is three times higher than that found in the nozzle slot, since it responds to the continuity equation and to the ratio between the passing area at the nozzle slots and the total sectional area of the tubes in the perforated plate.

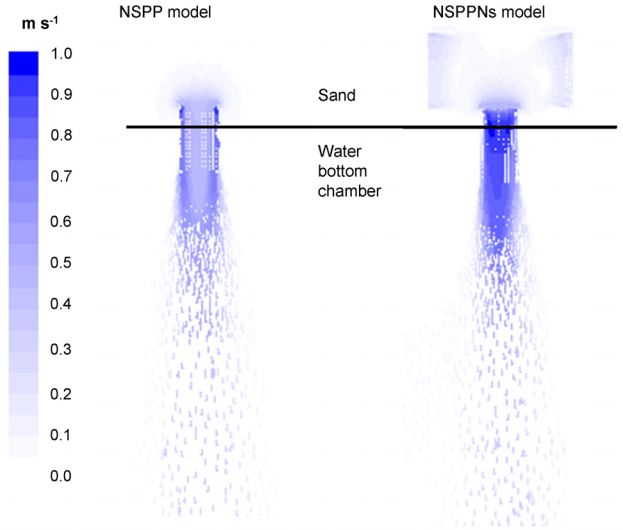

Figure 8. Velocity vectors (m s^{-1}) in a vertical cross-section through the tube (NSPP model) and nozzle symmetry plane (NSPPN$_s$ model).

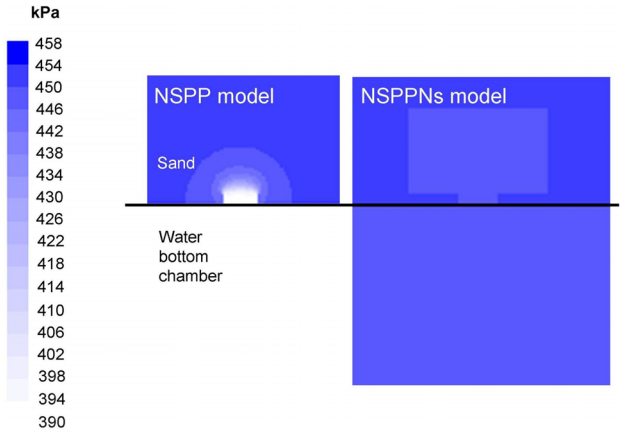

Figure 9. Pressure distribution (kPa) in a vertical cross-section plane through the tube (NSPP model) and nozzle symmetry plane (NSPPN$_s$ model).

Figure 9 shows the pressure distribution for the NSPP and NSPPN$_s$ models. In the NSPP model, the mean pressure in the tubes section was 390 kPa, while in the NSPPN$_s$ model it was 450 kPa. This can be explained by the velocity at the sand bed being reduced in the NSPPN$_s$ model (fig. 8) and therefore the head losses being lower when the effect of the nozzle is included. In addition, the velocity magnitude pattern found near the tube within the sand volume in the NSPP model leads to a highly nonuniform pressure distribution on the surface area at the tube entrance. This implies a velocity profile within the tube that substantially differs from that of the NSPPN$_s$ model (fig. 8), where an almost uniform pressure distribution at the tube entrance was found (fig. 9).

Thus, the application of the CFD software shows the effect of nozzles on reducing head losses when compared with results obtained for a hypothetical filter without nozzles. This could help to diagnose the effects of damage to or the detachment of a nozzle, which would produce an abrupt increase in head losses.

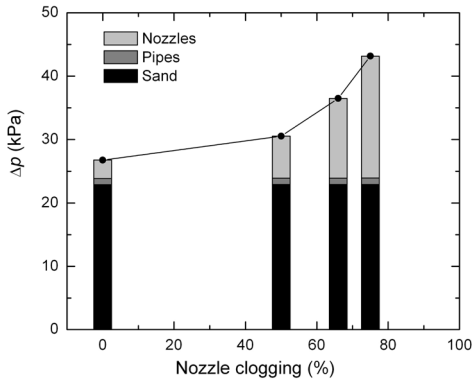

Figure 10. Total head losses (Δp_t) and head losses in the sand media, pipes, and nozzle for different degrees of filter clogging.

Effect of Nozzle Clogging on Head Losses

Based on the NSPPN$_s$ model, four degrees of nozzle clogging (0%, 50%, 66%, and 75%) were studied. The clogging consisted of completely blocking water passing through some of the nozzle slots, distributed among different nozzles. In figure 10, the total head losses for each clogging level are depicted. As shown, head losses were 23 kPa at the sand bed and 1 kPa at the inlet and outlet pipes and were almost independent of the clogging level. Head losses at the nozzles for clogging of 0%, 50%, 66%, and 75% were respectively 2.7, 6.5, 12.0, and 21.1 kPa, meaning that the increase in the head losses with the degree of clogging was not linear. When 66% of the total slots in the nozzles were clogged, the total passing area of the tubes in the perforated plate and the total nozzle slot area were approximately the same. But the total head losses when 66% of the slots were clogged was 36 kPa (fig. 10), significantly smaller than in the idealized case without a nozzle, as considered in the NSPP model, where the total head losses were 82 kPa (fig. 5). The greater head losses in the NSPP model compared with the NSPPN$_s$ model with 66% clogging of slots shows the importance of nozzles in head losses, as was discussed in the previous section when both the NSPP and NSPPN$_s$ models were compared.

The results also indicate that when the degree of clogging went over 50%, head losses increased dramatically (fig. 10). When 75% of the total slots of the nozzles were clogged, total head losses reached 45 kPa, which is close to the value used to initiate the automatic backwashing of the sand filter. A practical consequence, in an automatic backwashed filter, would be that when the clogging level in the nozzles increased by 50%, frequent automatic backwashing would be generated even if the sand bed was completely free of deposits. Indeed, Fahjen (1995) has already pointed out that the malfunctioning of a sand filter can be caused by the clogging of nozzles even when the filter bed is in perfect condition.

Modifying Current Nozzle Design

A new nozzle design was based on the cylindrical nozzles of the NSPPN$_s$ model. The modification consisted of increasing the number of slots from 20 to 30; therefore, the open area per nozzle increased by 50% compared with that of the NSPPN$_s$ model. As was demonstrated, when a nozzle was partially clogged, an increase in the ratio between the passing area through the nozzle slots and the passing area

Table 3. Comparison between partial and total pressure head losses in the newly designed nozzles and partial and total head losses in the $NSPPN_s$ model.

	New Nozzle Design	$NSPPN_s$	Change (%)
Head loss in nozzles (Pa)	2097	2898	-27.6
Head loss in pipes (Pa)	992	983	0.9
Head loss in sand media (Pa)	22856	22886	0.1
Total head loss (Pa)	25945	26762	-3.1

through the pressure plate had an effect on the total head losses. The results of using a new nozzle design are shown in table 3. A 28% reduction in head losses in the nozzle was found with the new design, although total head losses were only reduced 3%. According to figure 10 for 0% nozzle clogging, head losses through nozzles contribute 10.8% of the total value, so optimizing the nozzles by increasing their passing area has little effects on the total head losses when all the slots are fully opened. Nevertheless, an increase in the number of slots per nozzle could delay the clogging effects and thus be useful in preventing the problems associated with clogging described in the previous section.

Conclusions

A CFD model was used to simulate the hydraulic behavior of a sand filter for a microirrigation system and to predict the head losses in different elements in the filter (sand media and auxiliary elements). Simulation with models of different complexity indicated that 84.6% of the head losses were located in the sand media. The rest of the head losses were produced in the auxiliary elements, with 11.0% in the nozzles and perforated plate and 4.4% in the inlet and outlet pipes. The more realistic filter model ($NSPPN_a$) predicted head losses closest to the experimental data, being 8% smaller that the measured value.

The results of the different CFD models showed the importance of the nozzles in the filter's hydraulic behavior. The water chamber formed and the modification of the stream lines reduced head losses when the nozzle was present in comparison with a hypothetical sand and perforated plate configuration (without nozzles). The relationship between the passing area of the nozzles and the passing area of the perforated plate is an important design parameter. It is 3:1 in current filter design. A reduction in this relationship to simulate partial clogging of the nozzles showed that head losses increased dramatically when the clogging was over 50%, and thus the relationship between the areas rose to more than 1.5:1. An increase in the degree of clogging to over 50% would produce an increase in automatic backwashing frequency even if the sand bed was completely free of deposits.

A new nozzle design consisting of an increase in the number of slots per nozzle (thereby increasing the relationship between the passing area of the nozzles and the passing area of the perforated plate) showed little effect on total head losses. However, it may be beneficial in reducing the risks associated with nozzle clogging. Another practical consequence for the diagnosis of filter malfunctioning derived from the simulation results was that an abrupt increase in total head losses could be caused by damage to or detachment of a nozzle.

Acknowledgements

The authors would like to express their gratitude to the Spanish Ministry of Education and Science for its financial support of this study through grants CGL200909342/BTE, CGL200802832/BTE, FIS200913050; to the Autonomous Government of Catalonia for grant 2009SGR374; and to the European Commission for grant NEST28192FEPRE. The authors would also like to thank Regaber and the Municipality of Celrà for their help in carrying out this investigation.

References

AWWA. 2001. AWWA standard for granular filter material. ANSI/AWWA B10001. Denver, Colo.: American Water Works Association.

Barth, K. 1995. Damages at filter nozzles and possibilities of their prevention. *GWF Wasser/Abwasser* 136(10): 531–535.

Burt, C. M. 2010. Hydraulics of commercial sand media filter tanks used for agricultural drip irrigation. ITRC Report No. R 10001. San Luis Obispo, Cal.: Irrigation Training and Research Center.

Burt, C. M., and S. W. Styles. 2007. Chapter 10: Filtration (solids removal). In *Drip and Micro Irrigation Design and Management for Tress, Vines, and Field Crops: Practice Plus Theory*, 175–222. C. M. Burt and S. W. Styles, eds. San Luis Obispo, Cal.: Poor Richard Press.

Celik, I. B., U. Ghia, P. J. Roache, C. J. Freitas, H. Coleman, and P. E. Raad. 2008. Procedure for estimation and reporting of uncertainty due to discretization in CFD applications. *ASME J. Fluids Eng.* 130(7): 1–7.

Duran-Ros, M., J. Puig-Bargués, G. Arbat, J. Barragán, and F. Ramírez de Cartagena. 2008. Definition of a SCADA system for a microirrigation network with effluents. *Comput. Electron. Agric.* 64(2): 338–342.

Duran-Ros, M., G. Arbat, J. Barragán, F. Ramírez de Cartagena, and J. Puig-Bargués. 2010. Assessment of head loss equations developed with dimensional analysis for mic-ro irrigation filters using effluents. *Biosystems Eng.* 106(4): 521–526.

Fahjen, W. 1995. A method for the rapid rehabilitation of clogged nozzles of rapid sand filters by the application of chemicals. *GWF Wasser/Abwasser* 142(8): 571–574.

Fluent. 2009. *Fluent User's Guide.* Ver. 6.3. Canonsburg, Pa.: ANSYS, Inc.

Macdonald, I. F., M. S. ElSayed, K. Mow, and F. A. L. Dullien. 1979. Flow through porous media: The Ergun equation revisited. *Ind. Eng. Chem. Fundam.* 18(3): 199–208.

Mataix, C. 1982. Chapter 11: Minor losses in ducts (in Spanish). In *Mecánica de Fluidos y Máquinas Hidráulicas*, 236–253. 2nd ed. Mexico D.F., Mexico: Oxford University Press.

Nakayama, F. S., B. J. Boman, and D. J. Pitts. 2007. Chapter 11: Maintenance. In *Microirrigation for Crop Production: Design, Operation, and Management*, 389–430. F. R. Lamm, J. E. Ayars, and F. S. Nakayama, eds. Amsterdam, The Netherlands: Elsevier.

Ortiz-Arroyo, A., F. Larachi, B. P. A. Grandjean, and S. Roy. 2002. CFD modeling and simulation of clogging in packed beds with nonaqueous media. *AICHE J.* 48(8): 1596–1609.

Palau-Salvador, G., L. H. Sanchis, P. GonzálezAltozano, and J. ArvizaValverde. 2006. Real local losses estimation for online emitters using empirical and numerical procedures. *J. Irrig. Drain. Eng.* 132(6): 522–530.

Provenzano, G., P. Di Dio, and G. Palau-Salvador. 2007. New computational fluid dynamic procedure to estimate friction and local losses in coextruded drip laterals. *J. Irrig. Drain. Eng.* 133(6): 520–527.

Puig-Bargués, J., J. Barragán, and F. Ramírez de Cartagena. 2005. Development of equations for calculating the head loss in

effluent filtration in microirrigation systems using dimensional analysis. *Biosystems Eng.* 92(3): 383–390.
Puig-Bargués, J., G. Arbat, M. Elbana, M. Duran-Ros, J. Barragán, F. Ramírez de Cartagena, and F. R. Lamm. 2010. Effect of flushing frequency on emitter clogging in microirrigation with effluents. *Agric. Water Mgmt.* 97(6): 883–891.
Pujol, T., J. Solà, L. Montoro, and M. Pelegrí. 2010. Hydraulic performance of an ancient Spanish watermill. *Renewable Energy* 35(2): 387–396.
Qian, F., and H. Wang. 2010. Study of the filtration performance of a plain wave fabric filter using response surface methodology. *J. Hazard. Mater.* 176(13): 559–568.
Qingsong, W., L. Gang, L. Jie, S. Yusheng, D. Wenchu, and H. Shuhuai. 2008. Evaluations of emitter clogging in drip irrigation by twophase flow simulations and laboratory experiments. *Comput. Electron. Agric.* 63(2): 294–303.
Ravina, I., E. Paz, Z. Sofer, A. Marcu, A. Schischa, G. Sagi, Y. Yechialy, and Y. Lev. 1997. Control of clogging with stored municipal sewage effluent. *Agric. Water Mgmt.* 33(23): 127–137.
Smith, P. L., Jr, and M. van Winkle. 1958. Discharge coefficients through perforated plates at Reynolds numbers of 400 to 3000. *AIChE J.* 4(3): 266–268.
Trooien, T. P., and D. J. Hills. 2007. Chapter 9: Application of biological effluent. In *Microirrigation for Crop Production: Design, Operation, and Management*, 329–356. F. R. Lamm, J. E. Ayars, and F. S. Nakayama eds. Amsterdam, The Netherlands: Elsevier.
Wei, Q., Y. Shi, G. Lu, W. Dong, and S. Huang. 2006. Study of hydraulic performance of the eddy channel for drip emitters. *Irrig. and Drainage* 55(1): 61–72.
White, F. M. 2008. Chapter 6: Viscous flow in ducts. In *Fluid Mechanics*, 382391. 6th ed. Boston, Mass.: Mc GrawHill.
Yurdem, H., V. Demir, and A. Degirmencioglu. 2008. Development of a mathematical model to predict head losses from disc filters in drip irrigation systems using dimensional analysis. *Biosystems Eng.* 100(1): 14–23.
Zaman, E., and P. Jalali. 2010. On hydraulic permeability of random packs of monodisperse spheres: Direct flow simulations versus correlations. *Physica A* 389(2): 205–214.

NOMENCLATURE

ASP = analytical model taking into account the head losses in the sand media and in the inlet and outlet pipes.
ASPP = analytical model taking into account the head losses in the sand media, the inlet and outlet pipes and the perforated plate.
NSP = numerical model taking into account the head losses in the sand media and in the inlet and outlet pipes.
NSPP = numerical model taking into account the head losses in the sand media, the inlet and outlet pipes and the perforated plate.
$NSPPN_s$ = numerical model taking into account the head losses in the sand media, the inlet and outlet pipes, the perforated plate and the simplified nozzle.
$NSPPN_a$ = numerical model taking into account the head losses in the sand media, the inlet and outlet pipes, the perforated plate and the actual nozzle.
p_A = pressure at the filter inlet (Pa)
p_B = pressure at the filter outlet (Pa)
p_{in} = measured pressure at the inlet filter collector (Pa)
p_{out} = measured pressure at the outlet filter derivation (Pa)
Q = volumetric flow rate ($m^3\ s^{-1}$)
Re = Reynolds number (dimensionless)
v_i = velocity vector for a sandless filter ($m\ s^{-1}$)
S_i = momentum source term ($N\ m^{-3}$)
α = permeability (m^2)
Δp = head loss (Pa)
Δp_i = head loss in inlet pipe (Pa)
Δp_M = major head loss (Pa)
Δp_m = minor head loss (Pa)
Δp_o = head loss in outlet pipes (Pa)
Δp_p = head losses in inlet and outlet pipes (Pa)
Δp_{pp} = head loss in the perforated plate (Pa)
Δp_s = head loss in the sand media (Pa)
Δp_t = total head loss in the sand filter (Pa)
ε = porosity of the sand (dimensionless)
ζ = minor loss coefficient (dimensionless)
μ = fluid viscosity (Pa s)
μ_T = turbulent fluid viscosity (Pa s)
ρ = fluid density ($kg\ m^{-3}$)